Computer-AidedDesign

Taylor & Francis
Taylor & Francis Group

Check for updates

Using collaborative robots to assist with travel path development for material deposition based additive manufacturing processes

Ana Djuric [a] and R. Jill Urbanic [b]

[a]Wayne State University, USA; [b]University of Windsor, Canada

ABSTRACT

Additive manufacturing process planning is in its infancy. Many new additive manufacturing plat-forms are being developed using a robotic based system for the positioning. It is proposed to use a collaborative robot solution to teach a 'median line' based travel path for a bead deposition based system to help with junction decision making. This input complements the model geometry and process planning settings. The logic for these tool paths is challenging algorithmically, but a process designer may have a solution in mind that it would be easier to teach; hence, integrating collaborative robots as part of the solution. Traditional robot systems require you to know the solution approach, while manual teaching involves intuition, and personal application experience. The collaborative robot is used with a designer as an intermediate step for rapid travel path development, as collaborative robots are designed for safe human-machine interactions. The designer generates path data via a collaborative robot, which is imported into process planning software. This 'proof of concept' work will be extended. The travel 'knowledge-based' data will be combined with the actual part geometry to develop a travel path using the input logic as a foundation.

1. Introduction

1.1. Additive manufacturing solutions

Additive manufacturing (AM), or 3D printing, is a man-ufacturing solution where a CAD model is sliced into layers, and each layer manufactured using 2D travel path solutions. The final component is the resultant of a set of stacked layers. Typically the outer boundary contour are created first (either by depositing material or apply-ing a heat source onto deposited material), and then a raster scan zig-zag pattern is used to fill the interior of the layer (Fig. 1). For thin walled components, simple con-tours may be stacked to create a 3D component (Fig. 2). The AM fabrication strategy is advantageous compared to this problem set, as there is significantly less material usage. For the hexagonal shape in Fig. 2, the deposited material is approximately 12.5% of a solid hexagon with the same perimeter contour or 8% of a cubic stock block. Consequently, the material deposition AM family of solu-tions introduces significant materials savings opportu-nities, especially for expensive, exotic metal alloys (i.e. superalloys, titanium, etc.).

There are powder bed based AM metal fabrication solutions that are commercially available (select laser sintering (SLS) or direct metal laser sintering (DMSL)), but these systems are enclosed, which limits their work envelope, and only one material is used. Due to these limitations, many metal bead based deposition systems are being developed by original equipment manufacturer (OEM) solution providers. Platforms for AM solutions are being established for laser cladding [14, 17], electron beam manufacturing [9], cold metal transfer [20], as well as welding processes such as metal inert gas (MIG) weld-ing. Multi-axis system configurations, which could be serial 6 axis robot or machine tool based, are being devel-oped for surface build-ups, component refurbishment, and component fabrication.

Unlike machining, there is limited software is avail-able for AM process planning. Many companies are hand programming their solutions, or editing machin-ing solutions. However, an AM deposition tool path is not the inverse of a contouring or pocket tool path. As heat cycling is occurring during the process (Fig. 3), AM processes have distinctive tool path requirements, and the solutions are unique for each material-machine-part geometry combination. There are challenges link-ing the bead geometry to a machine's process settings (travel speed, material feed rate, power input, etc.) to generate a desired bead. However, the due to the heat transfer, and the placement of prior beads, the bound-ary conditions are changing dynamically for bead stack-ing and overlapping scenarios. Consequently, along with
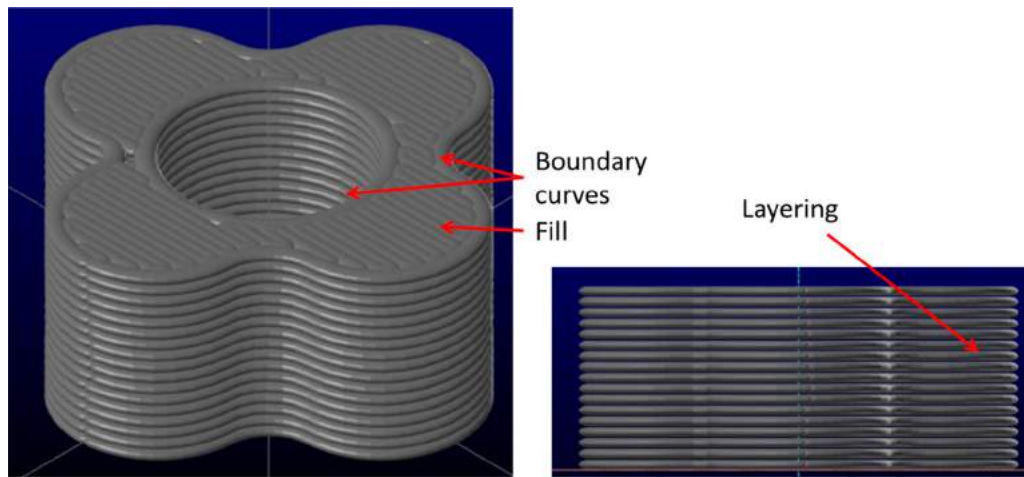
Figure 1. Virtual simulation of an additive manufactured component, illustrating the contour and fill tool paths, and the layering.
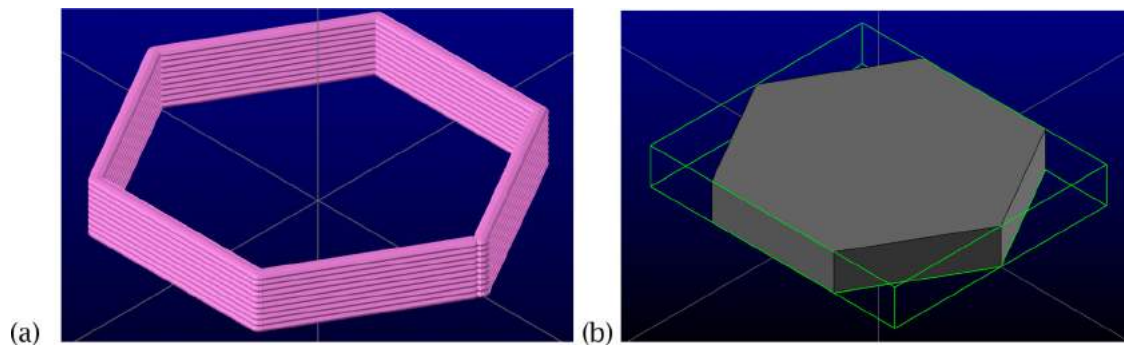
Figure 2. Virtual simulation of (a) a thin walled component, and (b) cubic stock boundary for a hexagonal block.
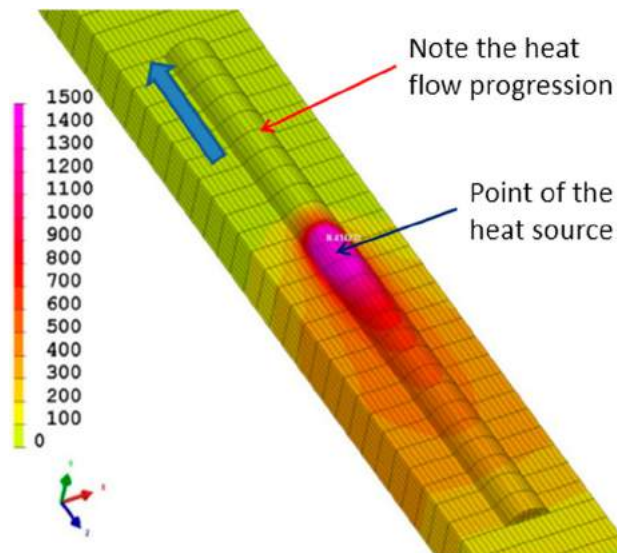
Figure 3. Heat progression simulation for a laser cladding bead (420 stainless steel) being deposited onto AISI 1018 mild steel [18].

the geometry-process setting challenges, there are issues with respect to understanding the resulting component properties, such as hardness and residual stresses.

Process planners developing these technologies have distinct ideas how to generate travel path solutions as they have knowledge and/or experience with the heat transfer and cycling conditions. The solutions will vary based on the part geometry, the heat source characteristics, and the material. For example, introducing internal ribs to the hexagon (Fig. 4) presents precedence issues at the intersection points, and flow directional issues.

The fundamental question is: how can AM metal deposition tool paths be created that are appropriate with respect to the problem being solved? Along with the process-material combinations, and their associated process challenges [22], there are multiple cases related to geometry that need to be considered, which are: (i) the size of the deposited bead to the geometry, (ii) corner filleting conditions, and the control logic that occurs at multi-point junctions. With machining, establishing an overlapping criterion is standard; however, interference conditions occur for metal (or thermoplastic / cement) beads. A 100% overlap would stack one bead on top of another.

When the bead size is smaller than the rib geometry, a contour and fill strategy will need to be employed. Multiple contours (Fig. 5 (a)) or a contour zig-zag fill
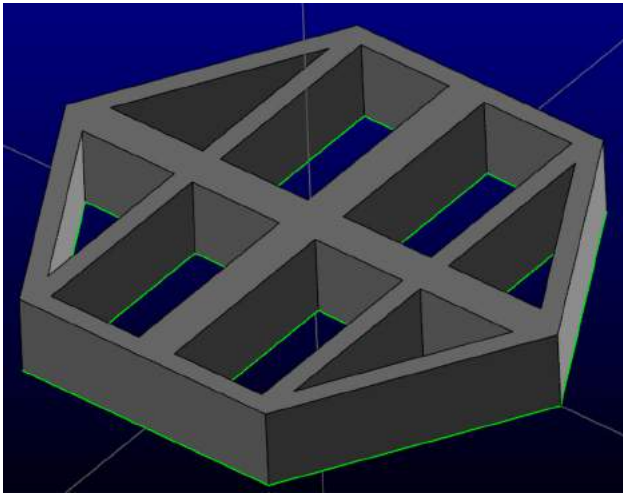
Figure 4. Boundary with variable thickness internal ribs.

(Fig. 5 (b)) would be a standard approach. However, for a bead thickness equal or greater than the model geometry, a median line needs to be established. For both cases, a tool path decision is required at each intersection point. Selected cases are illustrated in Fig. 5. The interactive planning decisions would consider the input heat (a path direction constraint), and the feasibility of starting and stopping the material feeding system (a discontinuity constraint).

The long term goal is using AM to fabricate near net metal shapes for subsequent machining. A path planning software framework and visualization tools are being developed in this area. Laser cladding and electron beam welding beads can vary between 2 – 10 mm. The power input from electron beam additive manufacturing (EBAM) may reach 42kW, whereas a cold metal transfer
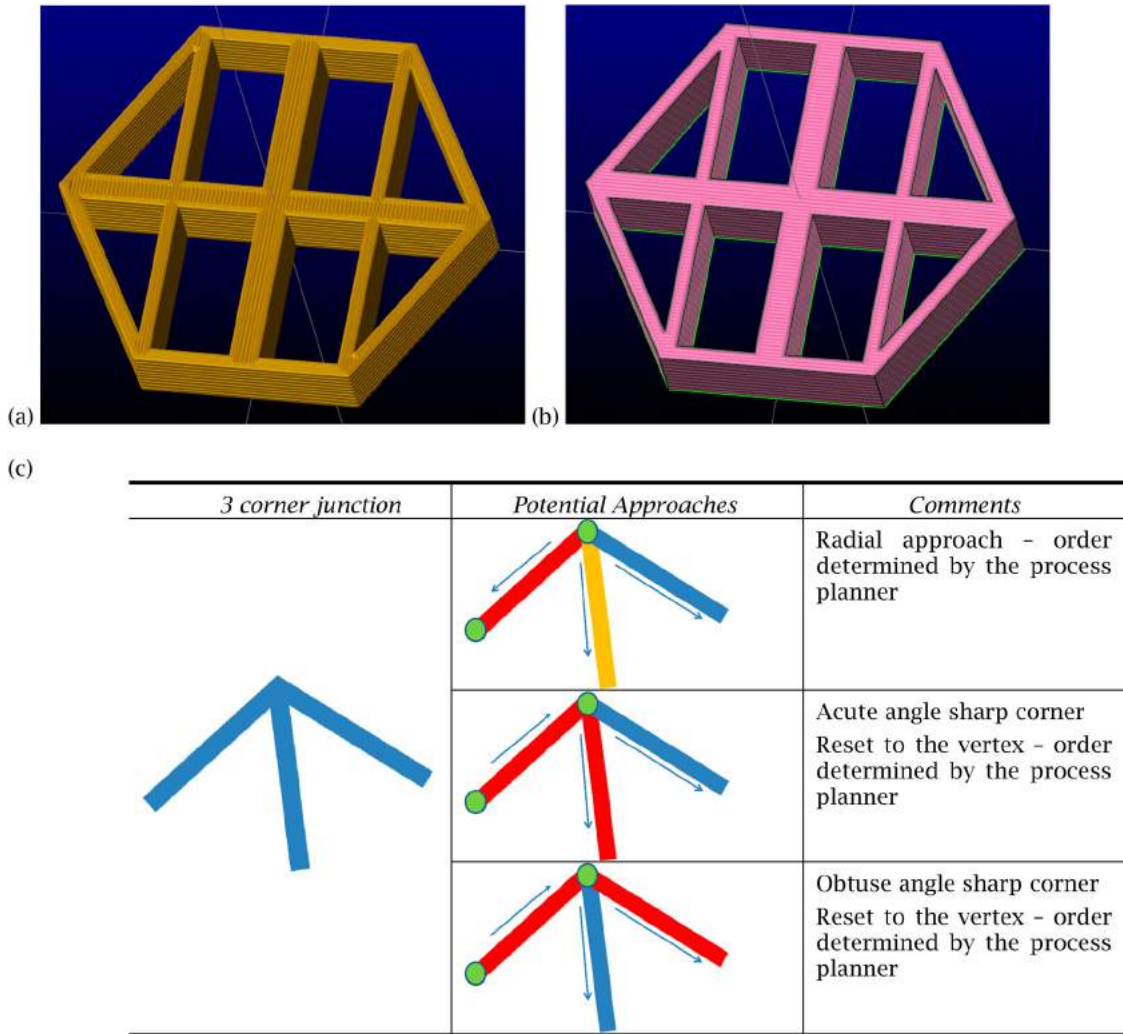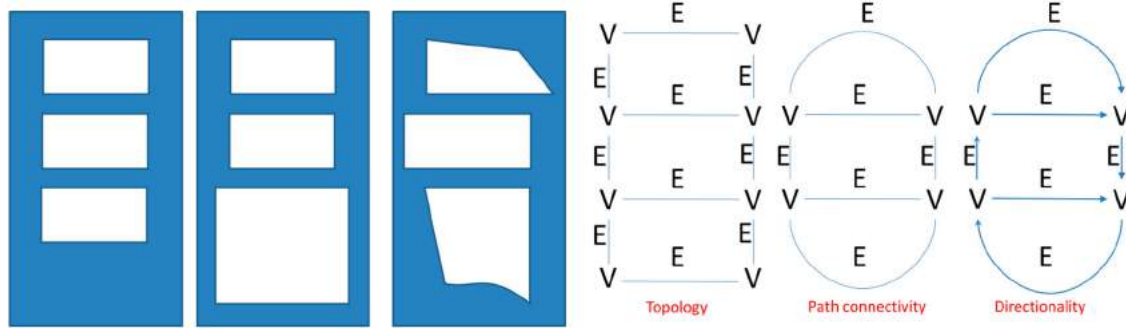

Figure 5. (a) 3 boundary curves with 50% overlap, and a 90° fill pattern, (b) 1 boundary curve, 50% overlap and a 0° fill pattern, and (c) tri-corner path planning decisions for sharp external vertices.

Figure 6. Structural relationships from a topology, path connectivity, and direction perspective, where V is a vertex, and E is an edge.

process can employ a standard 3 phase 220VAC power source. New thermoplastic systems are being developed to deposit 500 lbs (227 kg) of material per hour [16] and can have beads ∼ 5 mm thickness and 10–12 mm in width. This high volume deposition process also introduces unique process planning challenges related to heat and shrinkage. It can be seen that the material transfer and power requirements vary widely for AM material deposition processes.

In the next section, the logic challenges for junctions are presented. As aforementioned, experienced process planners know the preferred path strategy based on the heat input, heat flows, and the part geometry; however, presently they must create machining tool paths and modify them to suit. A method of 'teaching' a formalized tool path strategy needs to be developed to easily extract decision making information, which is the objective of this research. It is proposed to 'trace' a tool path using a collaborative robot and a representative drawing. This representative data set, which contains the decision logic, will be imported into a CAD/CAM software package, and adjusted to suit based on the actual geometry.

1.2. Structured decomposition

Graph theory is used to represent and code connections in an abstract structured manner. For the components shown in Fig. 6, the topology (or 'connections') is consistent for all cases, although the geometry is obviously different. The wall thicknesses and positions vary, but the basic edge-vertex connections are the same. There is different information when considering path relationships: a vertex occurs at a node where a decision related to a travel path must be made. However, when incorporating directionality, there is additional information to be considered. Priorities need to be established, i.e., traverse the interior geometry first, and then deposit material along the boundary, or traverse the edge geometry first, and then create specialty tool paths in the junction regions. There may be fillets in the corners, which will introduce

local issues even if the wall thicknesses are consistent in the component being fabricated (Fig. 7).

The tool path solution depends on the geometry, topology, path connectivity, and the directionality, and there are localized issues. The complexity is readily evident with these simple examples, although they are only 2D extrusion components. Introducing thick wall – thin wall junctions, draft, 3D fillets, and variable wall thicknesses increases the complexity as each layer must be analyzed. When machining, internal fillets for pockets are the default and are standard, as internal sharp corners are challenging to manufacture. A sink EDM or another specialty process is employed if this geometry is required. With AM processes, these standard fillet regions can be particularly problematic.

As decisions need to be made at the vertex junctions, motion control codes to indicate process start travel, stop travel, collect a data point, and rapid moves need to be established. This is under continuing development. Control codes related to the material feed rate, travel speed, contact tip to work piece distance, power levels, and so forth are related to the bead geometry and process type, and are established separately.

1.3. Collaborative robots

Collaborative robots (cobots) allow human operators to engage directly with this automation solution to realize enhanced performance. This advanced manufacturing technology solution is capable of transforming industrial automation [4, 10]. Cobots are designed to safely [4, 6, 7, 13, 15] and effectively interact with humans [1, 15, 21] while performing tasks independently or collaboratively within a shared workspace. Cobots are designed to be portable, and a key feature of this automation solution is that the programming has been simplified to consist of operator guidance, advanced hand held programming pads, or joysticks.

Human decision making is linked with the strength, robustness, durability, and dexterity of a robot. There
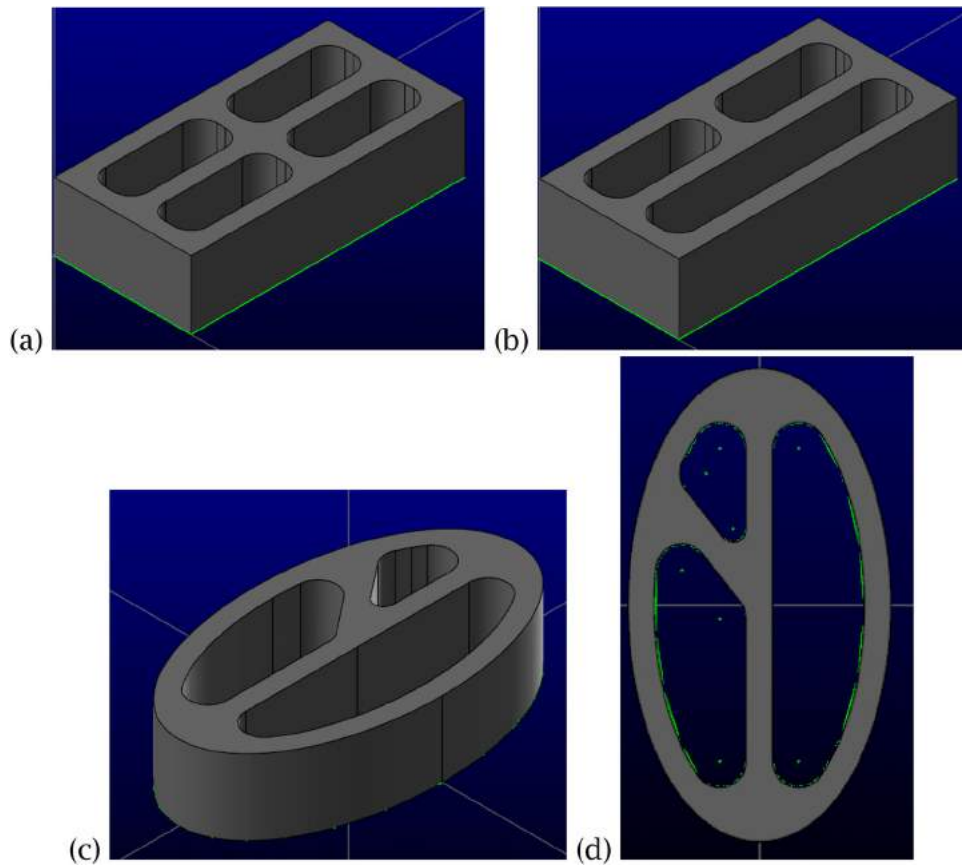
Figure 7. (a) and (b) various pockets with internal fillets, and external sharp corners, (c) and (d) curvy component with pockets, with a uniform wall thickness, which is influenced by the local internal fillets.

are several cobot solutions that exist (e.g., ABB FRIDA - YuMi, BOSCH – APAS, F&P Personal Robotics -Prob 1U, Yaskawa Motoman SDA10F dual-arm, Rethink Robotics –Baxter, and Universal Robots: UR3, UR5, and UR10). Researchers such as Anandan [1] predict 150,000 cobots are to be installed worldwide over the next three years. The Executive Summary World Robotics [10] predicts that double-digit growth of industrial robotics will happen between 2016 and 2019 and that linking the real-life factory with virtual reality will play an increasingly important role in global manufacturing.

Leveraging human and cobot synergies can only be realized when the cobot and human tasks are well-defined [11, 19, 21]. However, this does not mean that the tasks details are precisely known, exactly repeatable, and consistent. The ability to adapt to circumstances is a strength of this technology. They can adjust from application to application and can be quickly programmed for rapid repurposing [4]. For this work, the ease of using a cobot (Fig. 8) is leveraged as a teaching tool to capture an idealized tool path *strategy*. Unlike Antonelli and Astanin [2], who performed research with a collaborative robot in a welding cell, accuracy and repeatability are not an issue. In their work, the human actor handled the parts, and

taught the collaborative robot its path. Here, the goal is to have a planner trace out a path strategy and to extract decisions at junctions.

For this 'proof on concept', the Rethink Robotics –Baxter cobot is employed to capture the digital data for start and stop points, and travel directions. Joint angle data is extracted, and translated into the end effector X, Y, Z coordinates. This is suboptimal solution, but the Baxter cobot is employed for illustrating an advanced 'tracing' activity. For this research at this time, manual methods are employed.

2. Research methodology

A multi-phase research strategy has been developed for the general problem, as there is limited prior knowledge that has been published in this area (Fig. 9). First, the basic tool path travel problem is decomposed into sub-criteria: (i) topological assessment, (ii) path connectivity, and (iii) directionality (Fig. 6). A set of case studies are developed based on the physical scenarios, where the bead geometry is less than the geometry to be fabricated, equal to, or greater. As the long term goal of this work is to capture knowledge and transfer this into usable
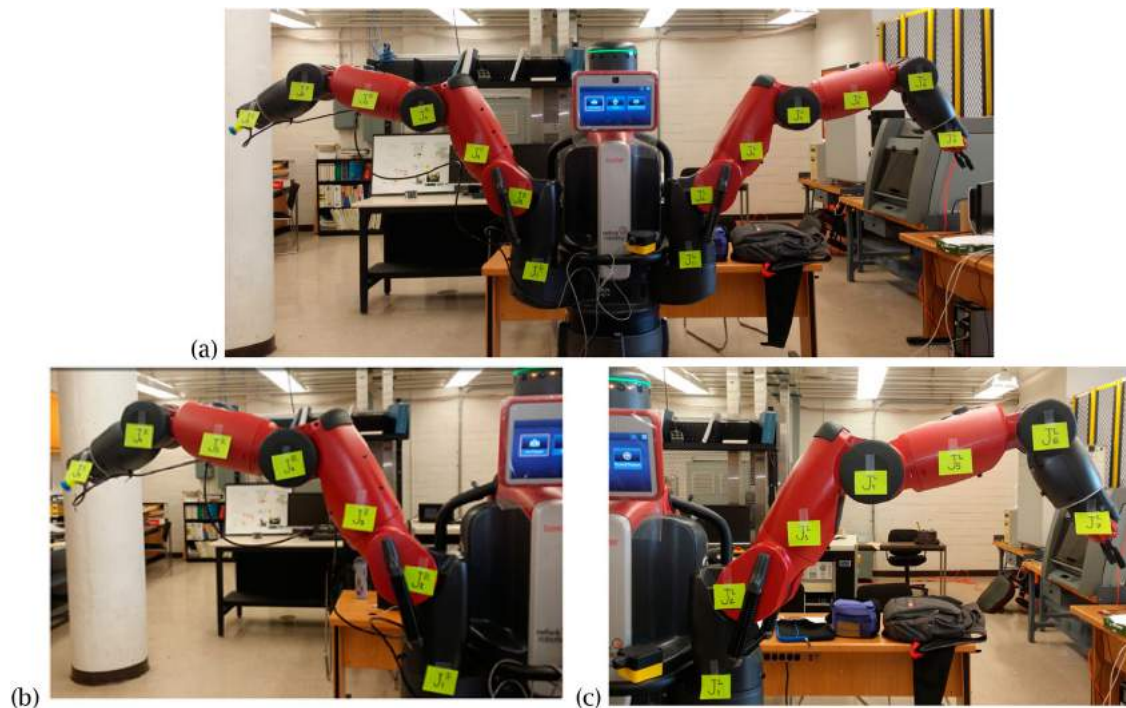
Figure 8. (a) Baxter robot, (b) right arm with joint labels, and (c) left arm with joint labels.
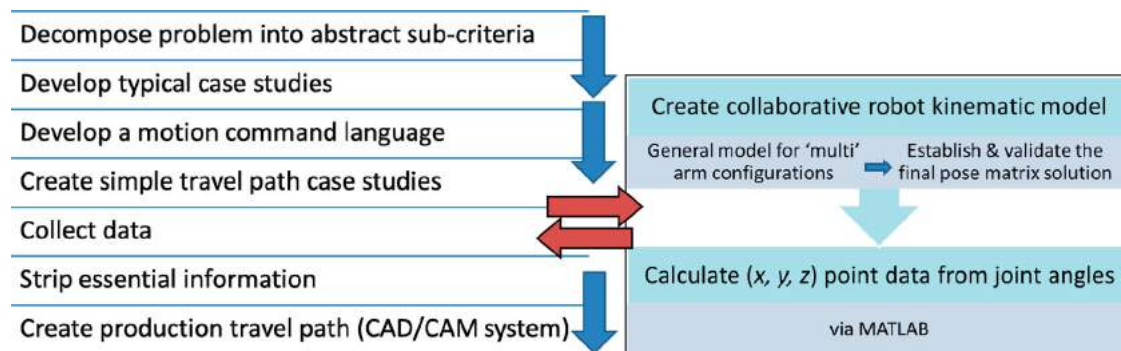
Figure 9. Research flow for this project.

data, a motion command language needs to be developed based on number of axes for the collaborative robot being employed for this work. For the initial experimentation, the Baxter robot [3 13] is manually guided by an operator to create a trajectory, which is perpendicular to the floor. As a decision strategy for junctions is desired, collision avoidance, vision systems, and other similar aspects considered by researchers is not required for this work [6, 11, 15].

The robot kinematic characteristics need to be developed using classic DH parameter kinematic modeling [5, 12]. The Baxter kinematic chains are illustrated in the Appendix A (Figure 16). For simple case studies (line, box, etc.), the collaborative robot is employed to create point / motion sets. Then the data needs to be collected, and the essential information stripped, and used as an input for the actual metal deposition travel path.

An additive process planning module developing using commercial CAD/CAM software is utilized for this last step.
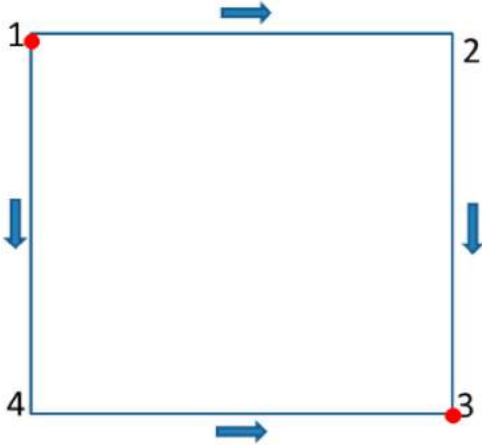
The control code motions are associated with the joint 7 (J7), and the initial set are summarized Tab. 1. This is under development.

Although tracing around a boundary is seemed to be the idealized solution; however, an alternative may be required depending on the process . Sample travel path flows for Fig. 10 are: (i) 123 reset (rapid move) 143 or (ii) 143 reset (rapid move) 123. The command structure for path (i) could include a continuous data stream, or the following:

- Start system at point 1
- Collect data at point 1
- Collect data at point 2

Table 1. Summary of initial base level motion control commands.

Command	Axis	Motion	Comment
Start	J7	CW orZ down	Power on, material feed for the systemSignal for data collection
Stop (power off, material feed)	J7	CCW orZ up	Power off, material feed for the systemSignal to conclude data collection
Rapid move	J7	Z up, traverse, Z down	Δx, Δy, Δz point between the two motions
Collect a data point	All	Z up, Z down	Topology information from the forward kinematic analysis

Table 2. Baxter Reconfigurable Kinematic Model Parameters.

Joint i	d_i	θ_i	a_i	α_i^L	α_i^R	Reconfiguration Parameters
1	d_1	$\theta_1^L = 0°, \theta_1^R = 180°$	a_1	$-90°$	$90°$	$K_1 = \sin\alpha_1$
2	0	$\theta_2^L = 90°, \theta_2^R = -90°$	0	$90°$	$-90°$	$K_2 = \sin\alpha_2$
3	d_3	$\theta_3^{LR} = 0°$	a_3	$-90°$	$90°$	$K_3 = \sin\alpha_3$
4	0	$\theta_4^{LR} = 0°$	0	$90°$	$-90°$	$K_4 = \sin\alpha_4$
5	d_5	$\theta_5^{LR} = 0°$	a_5	$-90°$	$90°$	$K_5 = \sin\alpha_5$
6	0	$\theta_6^{LR} = 0°$	0	$90°$	$-90°$	$K_6 = \sin\alpha_6$
7	d_7	$\theta_7^{LR} = 0°$	0	$0°$	$0°$	$K_7 = \cos\alpha_7$

Figure 10. Logic flows for a boundary.

- Collect data at point 3
- Stop system at point 3
- **Rapid** to point 1
- Start system at point 1
- Collect data at point 1
- Collect data at point 4
- Collect data at point 3
- Stop system at point 3

The representative points or point sets need to be collected that can be input into the planning software. The angle between points, z movements, etc. can be parsed, and input into the process planning software. The point generation method is discussed next.

The Baxter robot [3] has seven joints each, for a left and right arm (Appendix A). The kinematic model has been previously developed, and for a detailed analysis, refer to e Silva et al [8]. This unified model contains seven reconfiguration parameters: K_1, K_2, K_3, K_4, K_5, K_6, and K_7 (Tab. 2). Using kinematic theory, the Baxter joint values are converted to the World Frame (points' position and orientation). A sample of trajectory points are presented in Appendix B. Using the Matlab tools, the trajectory has been validated and visualized.

Using the new Baxter kinematic representation, the homogeneous transformation matrices are generated and forward kinematic has been obtained. See equations (1 and 2).

$$^0A_7^{LR} = {}^0A_1^{LR1}A_2^{LR2}A_3^{LR3}A_4^{LR4}A_5^{LR5}A_6^{LR6}A_7^R \quad (2.1)$$

Where $^0A_7^{LR}$ is the pose matrix of the unified Left and Right arms end-effector related to the base frame.

$$^0A_7^{LR} = \begin{bmatrix} n_x^{LR} & s_x^{LR} & a_x^{LR} & p_x^{LR} \\ n_y^{LR} & s_y^{LR} & a_y^{LR} & p_y^{LR} \\ n_z^{LR} & s_z^{LR} & a_z^{LR} & p_z^{LR} \\ 0 & 0 & 0 & 1 \end{bmatrix} \quad (2.2)$$

The experiment has been done for the Left arm by autogeneration of the forward kinematic solver for the Left arm reconfigurable parameters: $K_1 = -1$, $K_2 = +1$, $K_3 = -1$, $K_4 = +1$, $K_5 = -1$, $K_6 = +1$, $K_7 = +1$ For example, point 10 from Appendix B has Joints values (angles in radians). See equation 2.3.

$$\text{theta1\_Pendent} = -1.08682539;$$
$$\text{theta2\_Pendent} = -0.54072823;$$
$$\text{theta3\_Pendent} = 0.003451457;$$
$$\text{theta4\_Pendent} = 0.736694273; \quad (2.3)$$
$$\text{theta5\_Pendent} = -0.0080534;$$
$$\text{theta6\_Pendent} = 1.355272026;$$
$$\text{theta7\_Pendent} = -2.44784984;$$

Point 10 in the World Frame is presented in equation 2.4.

$$^0A_7^{L10} = \begin{bmatrix} -0.2050 & -0.9788 & 0.0048 & 366.3522 \\ -0.9786 & 0.2048 & -0.0196 & -697.5967 \\ 0.0182 & -0.0087 & -0.9998 & 35.4491 \\ 0 & 0 & 0 & 1 \end{bmatrix}$$
$$(2.4)$$

Where the position is described with X, Y and Z coordinates: 366.3522, −697.5967, and 35.4491, while the 3×3 matrix represents the orientation of the end-effector.
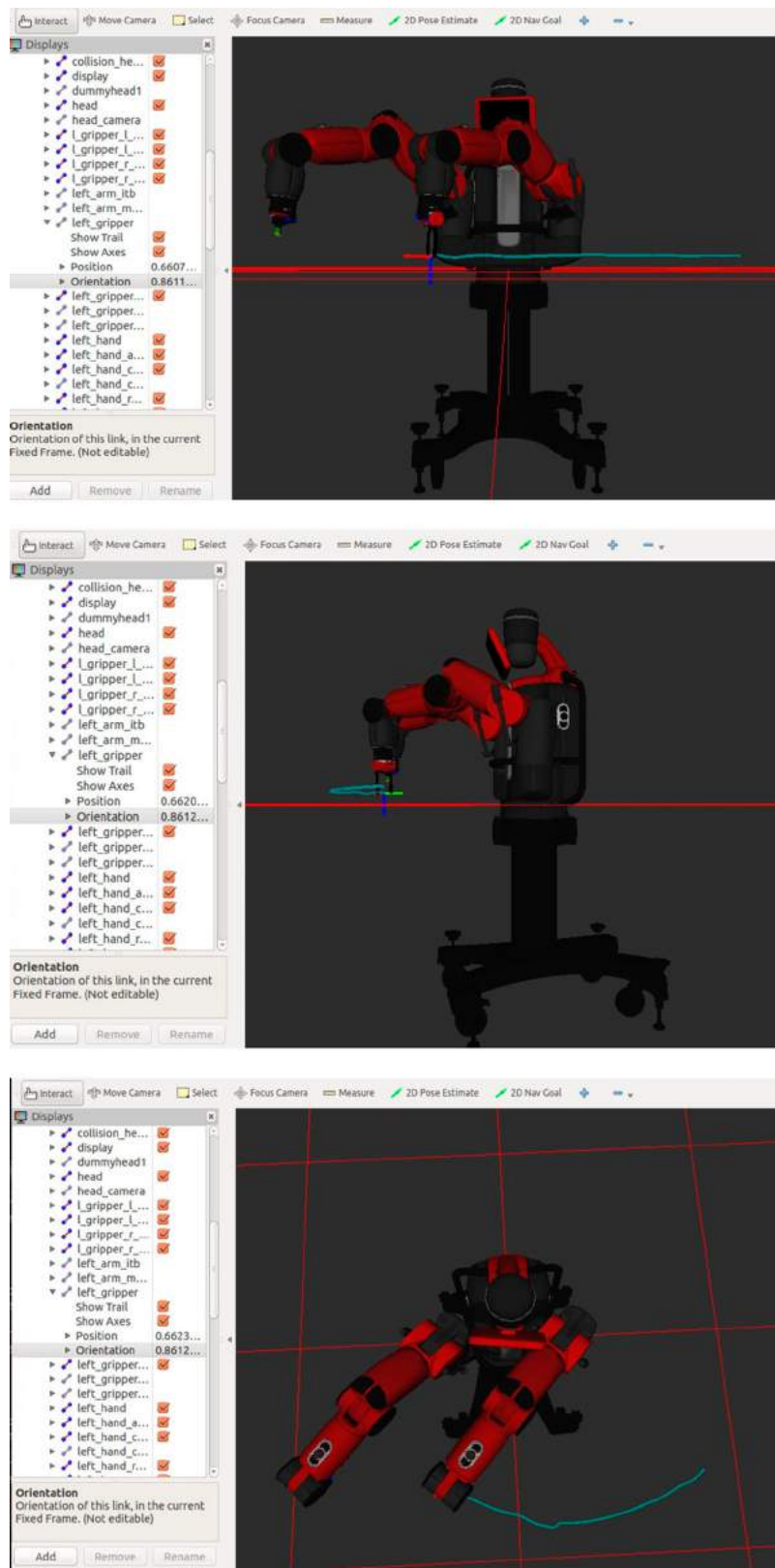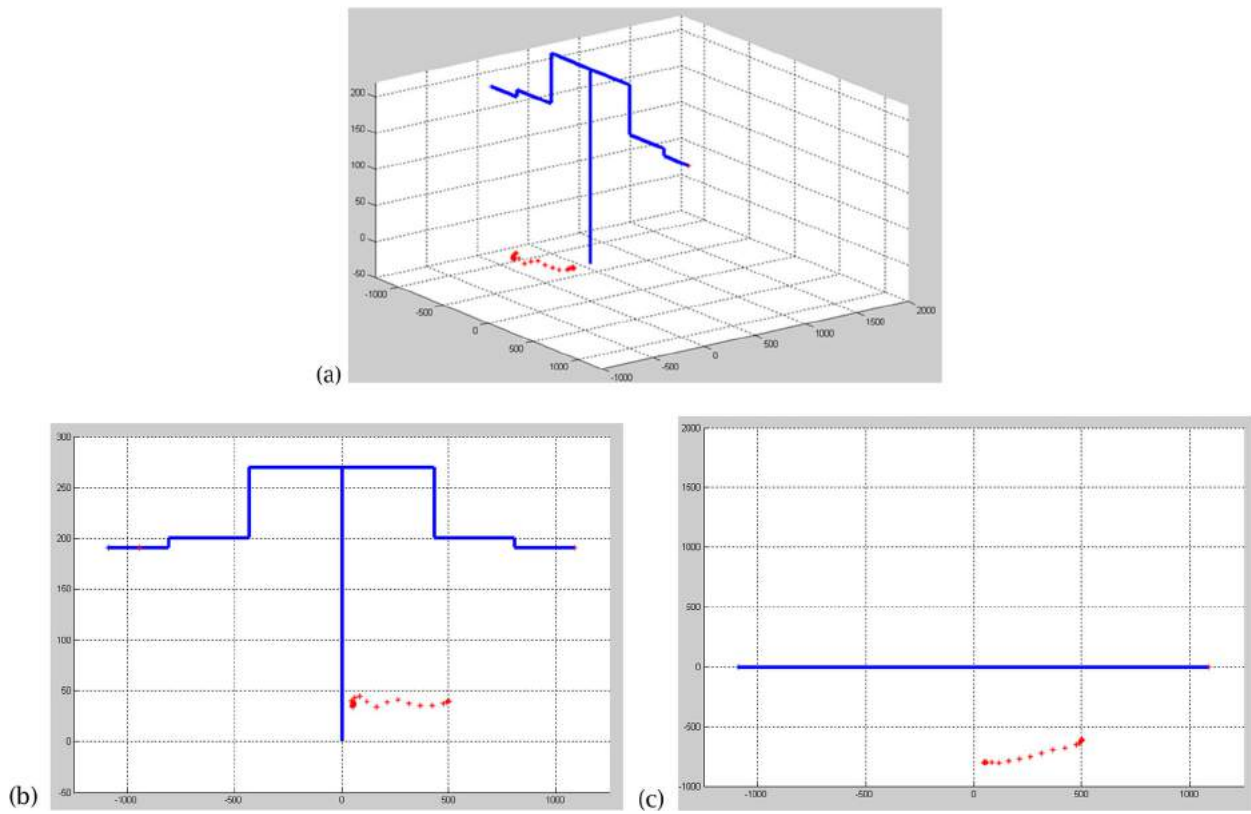
Figure 11. Various views for a trajectory.

Figure 12. (a) Isometric view, (b) front view, (c) top view of the trajectory. Note the 'wiggle'.
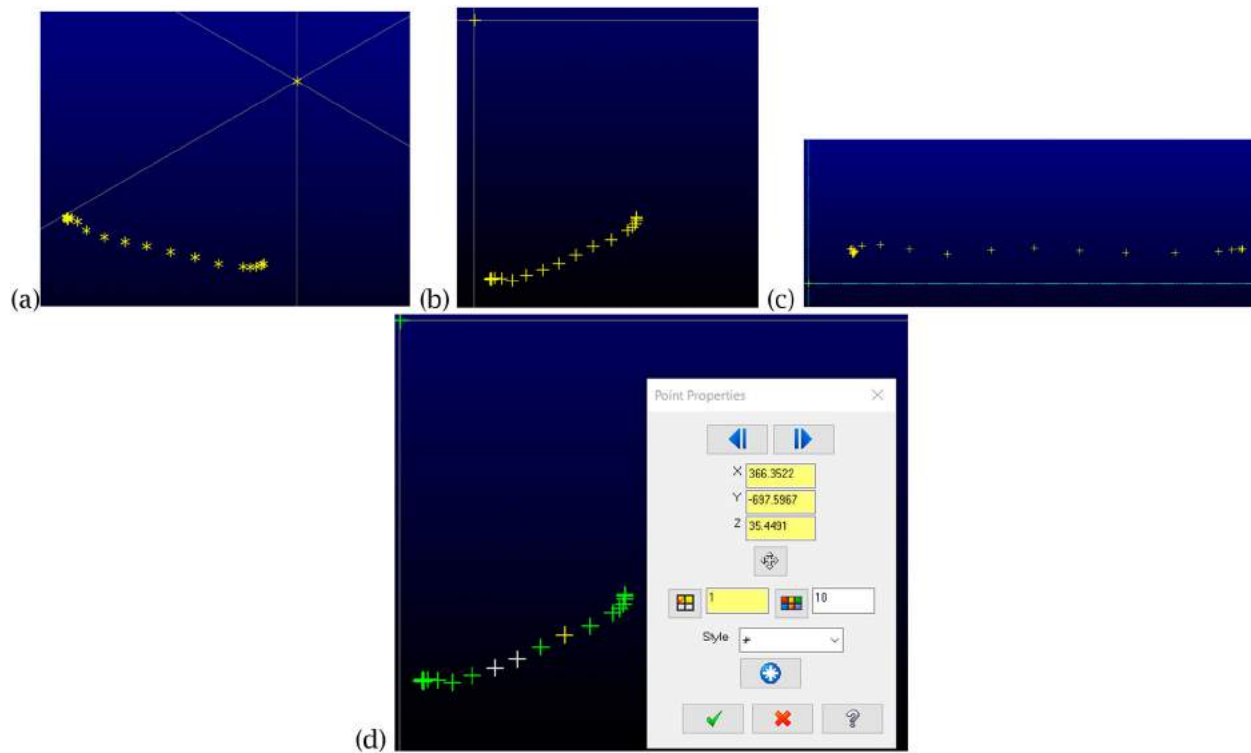

Figure 13. (a) Isometric view, (b) front view, (c) top view of the trajectory. Note the 'wiggle', (d) Point 10 position values in the CAD/CAM system.

3. Results

3.1. Linking the data to the CAD/CAM System

In Fig. 11, various views are provided which illustrate a trajectory path, and the data. The trajectory points are in Joint space and are expressed in radians. A set of points and the converted values are in Appendix A.

Using the Matalb tools, the trajectory has been validated and visualized (Fig. 12).

In 13 (a) and (b), the points, including the origin, are illustrated in the commercial CAD/CAM system. In Fig. 13 (c), the point 10 is highlighted and the coordinate data displayed. Consequently, the foundational links have been established.

3.2. Case study

As the communication has been established, a more complex shape, at two layers is explored (Fig. 14). The travel path created by the Baxter cobot is shown, along with an up-down z movement (encircled). A reduced data point set is extracted, and imported into the CAM software and displayed for one layer. The angle differentials, as well as the Δ z values are readily parsed and analysed (Tab. 3).

Tool path solutions for cases two and three in Fig. 5 (c) are illustrated in Fig. 15. The travel path for a component is sketched, the points collected in the desired order, and then imported into the Mathlab solution to generate the points. These points are then be imported into a commercial CAD/CAM program, and can be parsed and analysed

4. Summary and conclusions

In lieu of machining a block to result in a thin-walled component, thin walls can be built up using laser cladding or a similar process to generate a near net shape. Then this can be used as a stock model for
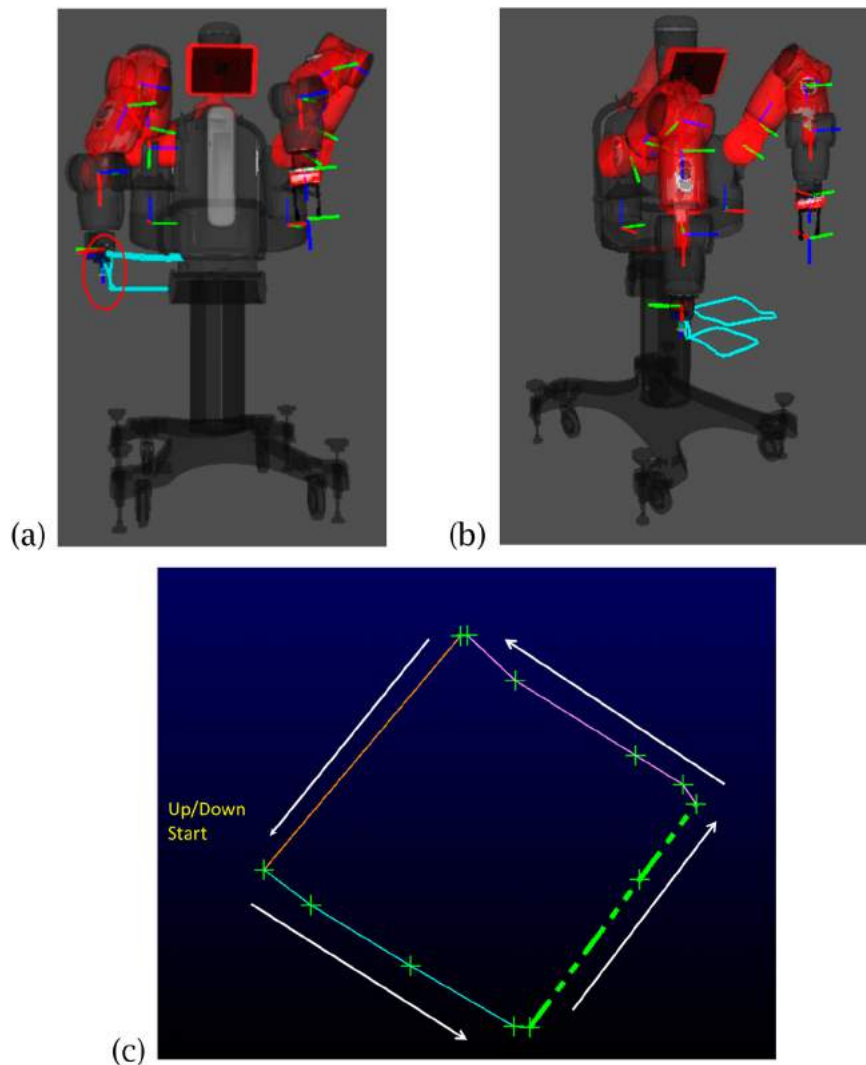
Figure 14. (a) and (b) Trajectory path and (c) selected points and the path direction in the CAM system.
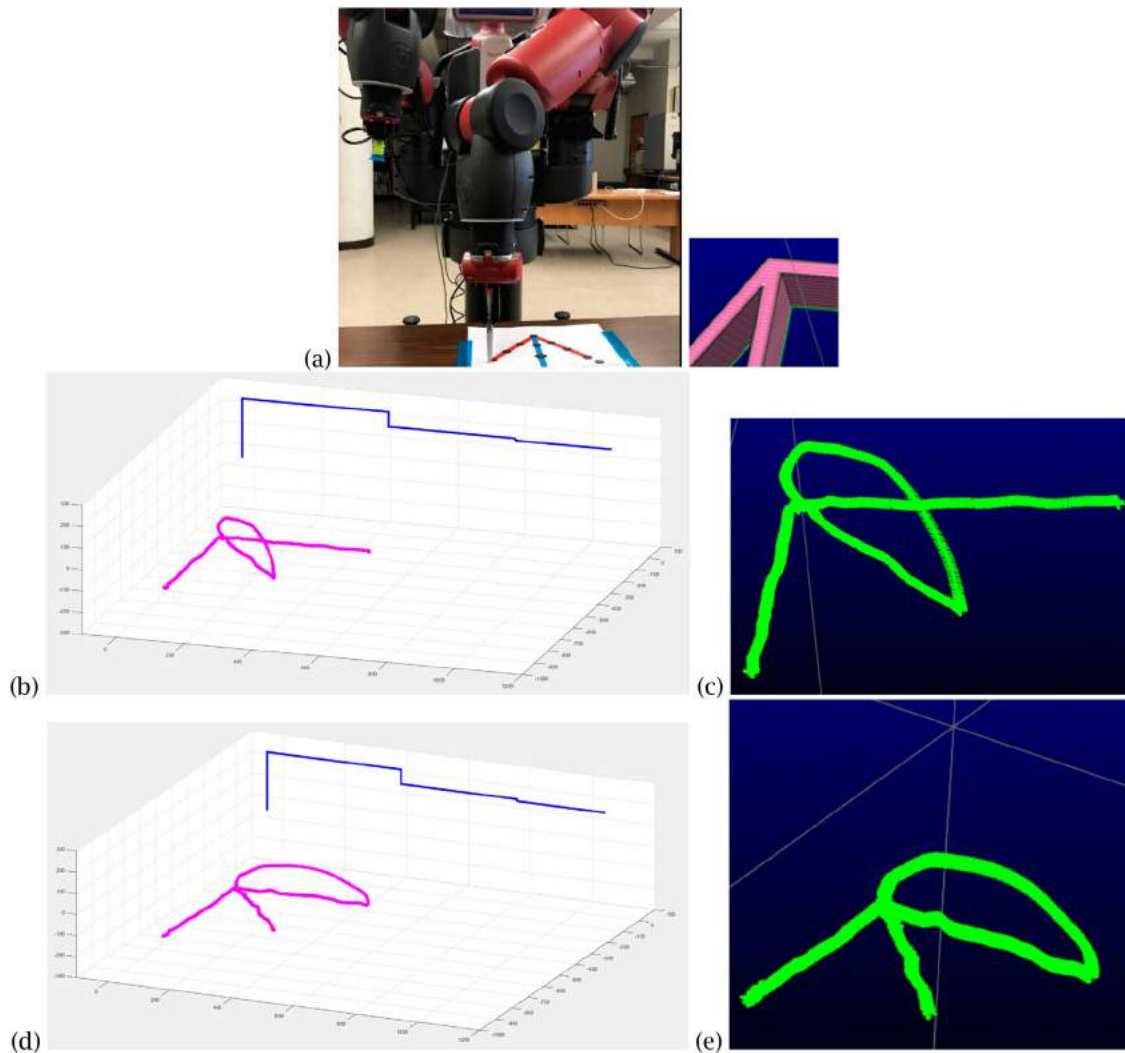
Figure 15. (a) Case 3 – a multi-junction scenario (data point collection illustrated at https://www.screencast.com/t/XB5Q8IEWpG), (b) the Matlab *x, y, z* coordinates for option 2, (c) CAD/CAM point set, (d) the Matlab *x, y, z* coordinates for option 3, (e) CAD/CAM point set.

Table 3. Selected point data, colour coded to match the geometry in Fig. 14 (c).

X	Y	Z	Angle between Points
−548.217	−469.935	173.9967	230
−516.788	−493.722	175.7902	323
−449.756	−534.5	175.7881	329
−380.436	−575.079	177.2472	330
−369.83	−575.855	177.0288	356
−296.097	−476.398	185.4146	53
−258.245	−425.865	189.6693	53
−266.945	−412.746	189.8633	124
−298.728	−393.187	187.9358	148
−379.745	−342.788	185.5688	148
−411.811	−312.418	185.9419	137
−416.181	−312.925	174.6812	230
−548.217	−469.935	173.9967	

finish machining. Establishing the appropriate relationships and the decision logic to automatically generate tool paths for multiple junction points, fillet regions, and variable wall thicknesses will depend on criteria such as

minimizing discontinuities, or stop and starts, or 'pushing' the heat in a certain direction, and is beyond the scope of any AM process planning software available today. Hence, it proposed to teach a representative travel path from a sketch or a printout of the CAD geometry, and parse the relevant point data and use this as a decision making input for actual travel path. If the essential information can be captured by a knowledgeable user and merged with tool path creation quickly, this would save considerable process planning time and effort.

The Baxter collaborative robot is employed to generate a trajectory, and this information is successfully imported into commercial CAD/CAM software. Downstream processing can be subsequently initiated. However, a simple trajectory contains several thousand points expressed in radians at each joint. The conversion process must be done offline as it was done here, or a solver must be implemented in the CAD/CAM software, and the full

kinematic solution must be utilized. Using a solver within the CAD/CAM environment will be the next step. Only preliminary work has been implemented at this time; however, now that the proof of concept has been established, this research will be extended to investigate a variety of junction scenarios and scalability, and to further automate the procedures between systems elements.

Acknowledgments

ORCID

Ana Djuric http://orcid.org/0000-0003-1257-9251
R. Jill Urbanic http://orcid.org/0000-0002-2906-7618

References

[1] Anandan, T.M.: The Realm of Collaborative Robots – Empowering Us in Many Forms, Robotic Industries Association, June 17, 2014.

[2] Antonelli, D.; Astanin, S.: Qualification of a collaborative human-robot welding cell, Procedia CIRP, 41, 2016, 352-7, https://doi.org/10.1016/j.procir.2015.12.036

[3] Baxter Research Robot Technical Specification Datasheet & Hardware Architecture Overview. Retrieved on 20th April 2016 From http://www.active8robots.com/wp-content/uploads/Baxter-Hardware-Specification-Architecture-Datasheet.pdf.

[4] Bloss, R.: Collaborative robots are rapidly providing major improvements in productivity, safety, programing ease, portability and cost while addressing many new applications, Industrial Robot, 43(5), 2016, 463-468, https://doi.org/10.1108/IR-05-2016-0148

[5] Corke I. P.: A Simple and Systematic Approach to Assigning Denavit-Hartenberg Parameters", IEEE Transaction on Robotics, 23(3), 2007, 590-594, https://doi.org/10.1109/TRO.2007.896765

[6] De Santis A.; Lippiello V.; Siciliano B.; Villani L.: Human – Robot Interaction Control Using Force and Vision, Adv. In Control Theory and Applications, LNCIS 353, 2007, 51-70.

[7] Djuric, A. M.; Urbanic, R. J.; Rickli, J.L.: A Framework for Collaborative Robot (CoBot) Integration in Advanced Manufacturing Systems, SAE International Journal of Materials and Manufacturing 9(2), 2016, 457-464, https://doi.org/10.4271/2016-01-0337

[8] e Silva, L.; Tennakoon, T.; Marques, M.; Djuric, A. M.: Baxter Kinematic Modeling, Validation and Reconfigurable Representation, SAE Technical Paper 2016-01-0334, 2016.

[9] Electron Beam Additive Manufacturing (EBAM™), url: http://www.sciaky.com/additive-manufacturing/electron-beam-additive-manufacturing-technology.

[10] Executive Summary World Robotics 2016 Industrial Robots http://www.ifr.org/fileadmin/user_upload/downloads/World_Robotics/2016/Executive_Summary_WR_Industrial_Robots_2016.pdf, accessed 25 October 2016.

[11] Faizal, S. A.; Ikeura, R.; Hayakawa, S.; Sawai, H.: Towards realizing collaborative rigid object transfer by a human hand and a robot manipulator, 2011 4th International Conference on Mechatronics: Integrated Engineering for Industrial and Societal Development, ICOM'11 - Conference Proceedings, 2011, Article number: 5937167, https://doi.org/10.1109/ICOM.2011.5937167

[12] Flanders M.; Kavanagh C. R.: Build-A-Robot: Using Virtual Reality to Visualize the Denavit-Hartenberg Parameters, Computer Applications in Engineering Education, 23, 2015, 846–853, https://doi.org/10.1002/cae.21656

[13] Haddadin S.; Suppa M.; Fuchs S.; Bodenmuller T.; Schaffer A. A.; Hirzinger G.: Towards a Robotic Co-Worker, Robotics Research, 2011, 261-282, https://doi.org/10.1007/978-3-642-19457-3_16

[14] Hybrid Manufacturing Technologies, Home url: http://www.hybridmanutech.com/.

[15] Kishi, Y.; Yamada, Y.; Yokoyama, K.: The role of joint stiffness enhancing collision reaction performance of collaborative robot manipulators, IEEE International Conference on Intelligent Robots and Systems, 2012, 376-381, https://doi.org/10.1109/IROS.2012.6385577

[16] LSAM, Large Scale Additive Manufacturing, url: http://www.thermwood.com/lsam_development_main.htm

[17] Mazak 2014, INTEGREX i-400AM, url: https://www.mazakusa.com/machines/integrex-i-400am/.

[18] Nazemi, N., Urbanic, R. J., A Finite Element Analysis for Thermal Analysis of Laser Cladding of Mild Steel with P420 Powder, Proceedings of the ASME 2016 International Mechanical Engineering Congress & Exposition IMECE2016-65654.

[19] Peshkin, M., Edward Colgate J., Cobots (invited), Industrial Robot, 26 (5), p. 335-341, 1999, https://doi.org/10.1108/01439919910283722

[20] Plus mfg (+MFG), Practical Metal Additive Manufacturing Equipment, Home url: http://plus-mfg.com/#section-about.

[21] Schröter, D.; Jaschewski, P.; Kuhrke, B.; Verl, A.: Methodology to Identify Applications for Collaborative Robots in Powertrain Assembly, Procedia CIRP - 5th CIRP Global Web Conference Research and Innovation for Future Production, 55, 2016, 12-17, 2016, https://doi.org/10.1016/j.procir.2016.08.015

[22] Urbanic, R. J., Hedrick, R., Burford, C., A process planning framework and virtual representation for bead-based additive manufacturing processes, International Journal of Advanced Manufacturing Technology, 90(361), 2016, DOI: doi:10.1007/s00170-016-9392-8; article is in-press.
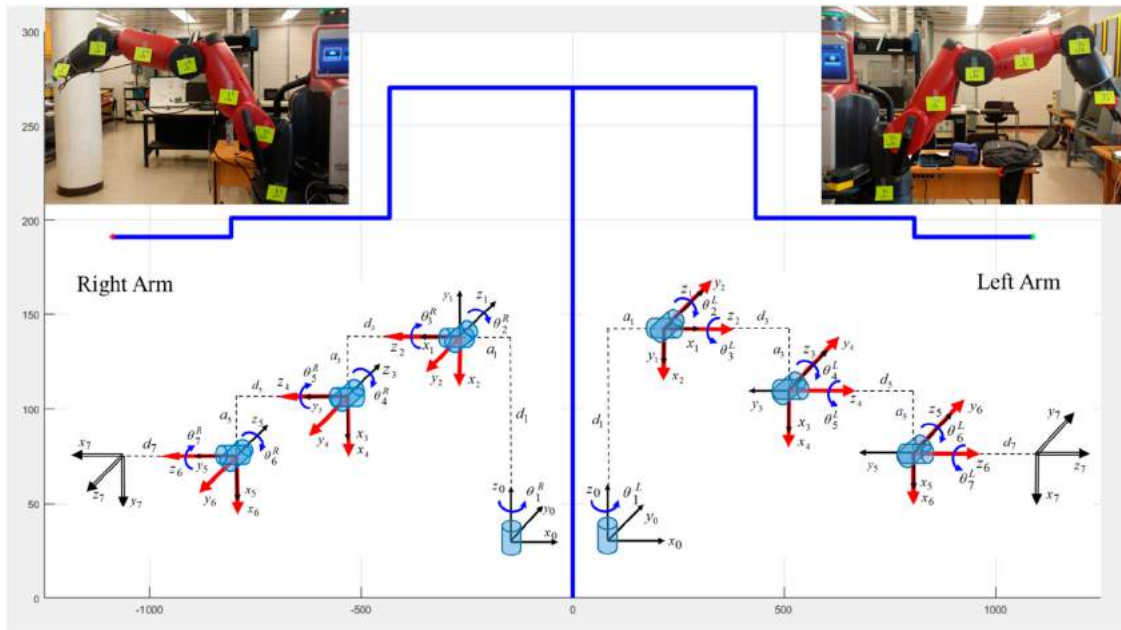
Appendix A

Figure 16. Baxter robot kinematic chain.

Appendix B

Trajectory points	Joint values (radians)	End-effector values (mm)			

1	theta1_Pendent = 0;
	theta2_Pendent = 0;
	theta3_Pendent = 0;
	theta4_Pendent = 0;
	theta5_Pendent = 0;
	theta6_Pendent = 0;
	theta7_Pendent = 0;
		0.0000
		0.0000
		−0.0010
		0
			−0.0000
			0.0010
			0.0000
			0
				0.0010
				0.0000
				0.0000
				0
					1.0880
					0.0000
					0.1910
					0.0010

2	theta1_Pendent = −0.86401468;
	theta2_Pendent = −0.54609716;
	theta3_Pendent = 0.003067962;
	theta4_Pendent = 0.738228254;
	theta5_Pendent = −0.05637379;
	theta6_Pendent = 1.361791444;
	theta7_Pendent = −2.01488376;
		−0.3952
		−0.9170
		0.0547
		0
			−0.9182
			0.3961
			0.0077
			0
				−0.0287
				−0.0472
				−0.9985
				0
					500.1831
					−607.6696
					39.1013
					1.0000

3	theta1_Pendent = −0.86401468;
	theta2_Pendent = −0.54609716;
	theta3_Pendent = 0.003067962;
	theta4_Pendent = 0.738228254;
	theta5_Pendent = −0.05637379;
	theta6_Pendent = 1.361791444;
	theta7_Pendent = −2.01488376;
		−0.3952
		−0.9170
		0.0547
		0
			−0.9182
			0.3961
			0.0077
			0
				−0.0287
				−0.0472
				−0.9985
				0
					500.1831
					−607.6696
					39.1013
					1.0000

4	theta1_Pendent = −0.86554866;
	theta2_Pendent = −0.54686415;
	theta3_Pendent = 0.003067962;
	theta4_Pendent = 0.737077769;
	theta5_Pendent = −0.05790777;
	theta6_Pendent = 1.353738045;
	theta7_Pendent = −2.05246629;
		−0.3615
		−0.9304
		0.0603
		0
			−0.9321
			0.3622
			0.0016
			0
				−0.0234
				−0.0557
				−0.9982
				0
					500.7907
					−610.8692
					40.1534
					1.0000

(continued).

Trajectory points	Joint values (radians)	End-effector values (mm)			

5	theta1_Pendent = −0.87206808;
	theta2_Pendent = −0.54686415;
	theta3_Pendent = 0.003451457;
	theta4_Pendent = 0.737077769;
	theta5_Pendent = −0.05407282;
	theta6_Pendent = 1.334946781;
	theta7_Pendent = −2.10692261;
		−0.3169
		−0.9461
		0.0662
		0
			−0.9484
			0.3168
			−0.0134
			0
				−0.0083
				−0.0671
				−0.9977
				0
					501.2272
					−617.2526
					40.2813
					1.0000

6	theta1_Pendent = −0.8862574;
	theta2_Pendent = −0.54648066;
	theta3_Pendent = 0.002684466;
	theta4_Pendent = 0.738228254;
	theta5_Pendent = −0.05062137;
	theta6_Pendent = 1.311553574;
	theta7_Pendent = −2.15485951;
		−0.2858
		−0.9552
		0.0766
		0
			−0.9583
			0.2843
			−0.0299
			0
				0.0068
				−0.0819
				−0.9966
				0
					496.7076
					−628.5723
					39.8915
					1.0000

7	theta1_Pendent = −0.90274769;
	theta2_Pendent = −0.54417968;
	theta3_Pendent = 0.002684466;
	theta4_Pendent = 0.737077769;
	theta5_Pendent = −0.05023787;
	theta6_Pendent = 1.298131242;
	theta7_Pendent = −2.20202942;
		−0.2563
		−0.9629
		0.0848
		0
			−0.9665
			0.2541
			−0.0364
			0
				0.0135
				−0.0913
				−0.9957
				0
					488.6508
					−639.4276
					38.9183
					1.0000

8	theta1_Pendent = −0.9265244;
	theta2_Pendent = −0.5426457;
	theta3_Pendent = 0.003834952;
	theta4_Pendent = 0.738611749;
	theta5_Pendent = −0.04601942;
	theta6_Pendent = 1.30388367;
	theta7_Pendent = −2.24459739;
		−0.2384
		−0.9681
		0.0768
		0
			−0.9711
			0.2368
			−0.0291
			0
				0.0100
				−0.0815
				−0.9966
				0
					473.2530
					−647.7532
					37.0132
					1.0000

9	theta1_Pendent = −1.01357781;
	theta2_Pendent = −0.54072823;
	theta3_Pendent = 0.003451457;
	theta4_Pendent = 0.738228254;
	theta5_Pendent = −0.00498544;
	theta6_Pendent = 1.313854545;
	theta7_Pendent = −2.38610712;
		−0.1949
		−0.9798
		0.0446
		0
			−0.9804
			0.1932
			−0.0393
			0
				0.0299
				−0.0514
				−0.9982
				0
					423.0199
					−677.7976
					35.3259
					1.0000

10	theta1_Pendent = −1.08682539;
	theta2_Pendent = −0.54072823;
	theta3_Pendent = 0.003451457;
	theta4_Pendent = 0.736694273;
	theta5_Pendent = −0.0080534;
	theta6_Pendent = 1.355272026;
	theta7_Pendent = −2.44784984;
		−0.2050
		−0.9786
		0.0182
		0
			−0.9788
			0.2048
			−0.0087
			0
				0.0048
				−0.0196
				−0.9998
				0
					366.3522
					−697.5967
					35.4491
					1.0000